DRAFT VERSION JULY 19, 2016
Preprint typeset using LaTeX style AASTeX6 v. 1.0

arXiv:1604.04631v2 [astro-ph.CO] 17 Jul 2016

STATISTICAL TEST OF DISTANCE-DUALITY RELATION WITH TYPE IA SUPERNOVAE AND BARYON ACOUSTIC OSCILLATIONS

CONG MA[1, 2, 3] AND PIER-STEFANO CORASANITI[3]

[1]Purple Mountain Observatory, Chinese Academy of Sciences, 2 West Beijing Rd, 210008 Nanjing, China
[2]Graduate School, University of the Chinese Academy of Sciences, 19A Yuquan Rd, 100049 Beijing, China
[3]LUTH, UMR 8102 CNRS, Observatoire de Paris, PSL Research University, Université Paris Diderot, 5 Place Jules Janssen, 92190 Meudon, France

Abstract

We test the distance-duality relation $\eta \equiv d_{\rm L}/[(1+z)^2 d_{\rm A}] = 1$ using cosmological luminosity distance ($d_{\rm L}$) from the JLA Type Ia supernovae compilation and angular-diameter distance ($d_{\rm A}$) based on BOSS and WiggleZ baryon acoustic oscillation measurements. The $d_{\rm L}$ measurements are matched to $d_{\rm A}$ redshift by a statistically-motivated compression procedure. By means of Monte Carlo methods, non-trivial and correlated distributions of η can be explored in a straightforward manner without resorting to a particular evolution template $\eta(z)$. Assuming *Planck* base-model cosmological parameter uncertainty, we find 3% constraints in favor of $\eta = 1$, consistent with the weaker 7–10% constraints obtained using WiggleZ data. These results stand in contrast to previous claims that $\eta < 1$ has been found close to or above 1σ level. We discuss the effect of cosmological parameter inputs on the results.

Keywords: cosmology: miscellaneous — distance scale — gravitation — methods: statistical

1. INTRODUCTION

A generic property of cosmological distances in General Relativity is that the angular-diameter distance $d_{\rm A}$ and the luminosity distance $d_{\rm L}$ to the same cosmological redshift z satisfy the distance-duality (DD) relation (Ellis 1971, 2009)

$$\eta \equiv \frac{d_{\rm L}(z)}{(1+z)^2 d_{\rm A}(z)} = 1. \qquad (1)$$

The theoretical underpinnings of this relation are the geometrical reciprocity relation (Etherington 1933, 2007) that holds in any metric theory of gravity, and the fact that photons propagate along null geodesics with the photon number conserved. This is not the case in non-metric theories of gravity, theories of varying fundamental constants, or axion–photon mixing models (Bassett & Kunz 2004; Uzan et al. 2004). Therefore, an observational falsification of Equation (1) can be a useful probe of exotic physics provided that cosmic distance measurements are exempt from astrophysical systematic errors (e.g. see Corasaniti 2006, for violations induced by inter-galactic dust extinction).

Several cosmological probes can be used for this purpose. Luminosity distances are indicated by the brightness of Type Ia supernovae (SNIa) through the standard candle relation, whereas angular-diameter distances can be inferred from the apparent size of cosmic standard rulers. Numerous studies devoted to testing the validity of Equation (1) have used SNIa $d_{\rm L}$ data in combination with $d_{\rm A}$ estimates from X-ray observations of galaxy clusters (e.g. Bassett & Kunz 2004; Uzan et al. 2004; de Bernardis et al. 2006; Holanda et al. 2010; Santos-da-Costa et al. 2015). However, astrophysical uncertainties such as the 3D profile of intra-cluster plasma may significantly affect the estimation of $d_{\rm A}$ (Meng et al. 2012; Yang et al. 2013). More reliable estimates can be derived from baryon acoustic oscillations (BAO) signal in the galaxy power spectrum that provides a measure of the ratio $d_{\rm A}/r_{\rm d}$, with $r_{\rm d}$ being the size of sound horizon at photon–baryon drag epoch. On the one hand, the cosmic microwave background (CMB) anisotropy power spectra tightly constrain the value of $r_{\rm d}$. On the other hand systematic effects due to the non-linearity of the matter density field alter $d_{\rm A}$ estimates to less than 1% level (Crocce & Scoccimarro 2008; Rasera et al. 2014).

A common approach to test the DD relation uses distance measurements to constrain parameterizations of η as a function of redshift z (e.g. Nair et al. 2012; Wu et al. 2015). The choice of a $\eta(z)$ template function imposes a strong prior on the DD analysis which may result in different outcomes depending on its form. In our view, a template-free falsification should be preferred since it also facilitate the identification of possible systematics.

A practical difficulty underlying the tests is the fact that measurements of $d_{\rm L}$ and $d_{\rm A}$ may not be available at the same redshift. Several studies have attempted to avoid this problem by selecting data points under a proximity criterion, e.g. by

cma@pmo.ac.cn
Pier-Stefano.Corasaniti@obspm.fr

only using data within a redshift separation $|\Delta z| \leq 5 \times 10^{-3}$ (Holanda et al. 2010). This incurs the cost of significantly reducing the statistical information encoded in the datasets. Moreover, it does not guarantee that the data points thus chosen provide a representative subsample. This situation is analogous to the problem of estimating the cross-correlation of unevenly sampled time-series data, for which narrow windows centered on cherry-picked data can lead to a spuriously high significance of detection (Max-Moerbeck et al. 2014).

To overcome the redshift-matching problem Cardone et al. (2012) have applied a local regression technique to the SNIa $d_{\rm L}$ data at redshift windows of interest with adjustable bandwidth. However, this method is not easily generalized to highly correlated data. It still rejects the majority of data points outside the narrow windows, and one might overlook their influence on $d_{\rm L}$ estimates through their systematic correlations with data points inside the windows.

The Joint Light-curve Analysis (JLA, Betoule et al. 2014) of SNIa has introduced a technique to compress correlated luminosity distance data at given control points in log-redshift space. This could have served as a solution to the z-matching problem, but unfortunately the compressed dataset contained artifacts due to incomplete statistical treatments of data covariance. In Ma et al. (2016, hereafter M16) we have detailed a Bayesian statistical method which corrects those errors and preserves information encoded in the full dataset.

Our goal is to provide up-to-date, straightforward, and independent measurements of η at selected redshifts, along with their correlations, using $d_{\rm L}$ from the compressed JLA dataset and $d_{\rm A}$ estimates from BAO measurements. In Section 2 we derive expressions for $d_{\rm L}$ and $d_{\rm A}$ in terms of the data. In Section 3 we describe our Monte Carlo (MC) analysis methods. The results are presented in Section 4 and discussed in Section 5.

2. DATASETS

2.1. *BAO Angular-Diameter Distance*

We use $d_{\rm A}$ estimates from BAO measurements of the WiggleZ survey (Blake et al. 2011a, 2012) and the Baryon Oscillation Spectroscopic Survey (BOSS) DR12 (Alam et al. 2016) consensus compilation. WiggleZ data consist of estimates of BAO volume distance parameter $A(z)$ (Eisenstein et al. 2005; Blake et al. 2011a) and the Alcock–Paczyński effect parameter $F(z)$ (Ballinger et al. 1996; Blake et al. 2011b) at effective redshifts 0.44, 0.60, and 0.73 respectively. The measurements can be combined to derive $d_{\rm A}$ through the following equation

$$d_{\rm A,WiggleZ}(z) = \frac{c}{H_0} \frac{A(z)[z^2 F(z)]^{1/3}}{\sqrt{\Omega_{\rm m}}(1+z)}, \tag{2}$$

where c is the speed of light, H_0 the Hubble constant, and $\Omega_{\rm m}$ the matter density parameter.

BOSS data on the other hand provide consensual estimates of the ratio $\widetilde{d}_M = d_{\rm A}(1+z) r_{\rm d}^{\rm fid}/r_{\rm d}$ by joining the constraints from BAO features and the full shape of galaxy correlations at effective redshifts 0.38, 0.51, and 0.61, where $r_{\rm d}^{\rm fid} = 147.78$ Mpc (Alam et al. 2016). Thus, we express $d_{\rm A}$ by

$$d_{\rm A,BOSS}(z) = \frac{r_{\rm d}}{r_{\rm d}^{\rm fid}} \frac{\widetilde{d}_M(z)}{(1+z)}. \tag{3}$$

We notice that the overlap of WiggleZ and BOSS survey volumes makes the two BAO datasets correlated (Beutler et al. 2016). However, a full analysis consistently joining the datasets is out of the scope of this letter. For this reason, when later in Section 4 we quote the results from these two datasets together, we do not imply they should be treated as if independent.

Evidently from Equations (2) and (3), to use BAO data we need to specify the cosmological parameters, or "complementary parameters" (CPs), namely $\boldsymbol{\varphi} = (H_0, \sqrt{\Omega_{\rm m}} H_0, r_{\rm d})$. The CPs are similar to the role of prior distributions in the context of inference problems, in that they are specified independently of and in complement to the data to express our belief or uncertainty. However, unlike prior distributions they cannot be updated by our process. In Section 3 we discuss the choice of such CPs.

2.2. *SNIa Luminosity Distance*

We compute compressed SNIa luminosity distance moduli $\mu_{\rm Lc}$ and their covariance matrix from the JLA dataset with the method detailed in M16. The redshifs of compression, or "control points", are chosen with two criteria in mind. Firstly, $\mu_{\rm Lc}$ must be available at the redshift of $d_{\rm A}$ data. Secondly, the control points should be distributed such that the statistical uncertainties on $\mu_{\rm Lc}$ are close to uniform. In practice, we perform two separate compression runs for SNIa + BOSS and SNIa + WiggleZ respectively. Each compressed dataset contains 15 suitably chosen control points between $0.01 \leq z \leq 1.30$, and the relevant data points are listed in Table 1. We have verified that the compression results are not affected significantly by the choice of the other control points.

Table 1. Compressed SNIa data at anchoring and BAO-matched control points.

z	$\mu_{\rm Lc}$
0.01	33.12 ± 0.05
SNIa + BOSS	
0.38	41.57 ± 0.03
0.51	42.30 ± 0.03
0.61	42.74 ± 0.03
SNIa + WiggleZ	

Table 1 continued

Table 1 *(continued)*

z	$\mu_{\rm Lc}$
0.44	41.93 ± 0.03
0.60	42.70 ± 0.03
0.73	43.21 ± 0.05

It should be noted that the compression step computes the distance moduli only up to an implicit magnitude offset M. It is the quantity

$$\mu_{\rm Lc} = \mu_{\rm L} - M = 5\log_{10}\left(\frac{d_{\rm L}}{10\ {\rm pc}}\right) - M \qquad (4)$$

that is produced by the compression. The parameter M in Equation (4) is degenerate with H_0 as discussed in M16 (see also Yang et al. 2013), and it is possible to eliminate M and to obtain $d_{\rm L}$ that is directly comparable to $d_{\rm A}$. We exploit the fact that at the lowest available, or the "anchoring" redshift $z_1 = 0.01$, the luminosity distance can be approximated to the second order as

$$d_{\rm L}(z_1) = \frac{cz_1}{H_0}\left[1 + \frac{1}{2}(1-q_0)\,z_1 + \mathcal{O}(z_1^2)\right] \approx \frac{cz_1}{H_0}, \qquad (5)$$

where q_0 is the deceleration parameter. For the small value of z_1 higher-order terms in Equation (5) are negligible (unless one must consider unrealistic cosmological scenarios with $|q_0| \approx 10^2$). This allows us to express M by $d_{\rm L}(z_1) \approx cz_1/H_0$ and $\mu_{\rm Lc}(z_1)$ using Equation (4). Carrying out the algebra, we obtain the expression for $d_{\rm L}(z)$ as

$$d_{\rm L}(z) = \left(\frac{cz_1}{H_0}\right) 10^{[\mu_{\rm Lc}(z) - \mu_{\rm Lc}(z_1)]/5}. \qquad (6)$$

3. METHODS

We estimate the probability density functions (PDFs) of η by computing η using MC samples of $d_{\rm L}$ and $d_{\rm A}$.

As discussed in Section 2.1, in the case of BAO data we need to account for the dependence on the CPs $\boldsymbol{\varphi} = (H_0, \sqrt{\Omega_{\rm m}}H_0, r_{\rm d})$, while for SNIa data we need to propagate the dependence on H_0. For this purpose we use the posterior Markov chains of the flat ΛCDM "base" model obtained from the *Planck* TT + low-ℓ temperature and polarization ("lowP") power spectrum data (Planck Collaboration et al. 2015). These CP samples are independent of the sampling of data random variables $(A, F, \widetilde{d}_M, \mu_{\rm Lc})$ detailed as follows.

For WiggleZ data, we generate a Gaussian sample of (A, F) using the mean vector and covariance matrix of Blake et al. (2012), marginalizing over the growth rate parameter $f\sigma_8$. By combining them with the CP samples through Equation (2) we obtain the sample of $d_{\rm A,WiggleZ}(z)$.

In the case of BOSS data, a Gaussian sample of $\widetilde{d}_M$ is created using the mean and covariance values of Alam et al. (2016), marginalizing over the $r_{\rm d}$-scaled expansion rate $(r_{\rm d}/r_{\rm d}^{\rm fid})H$ and the growth rate. Then, by combining through Equation (3) the $\widetilde{d}_M$ sample with that of $r_{\rm d}$ we obtain the $d_{\rm A,BOSS}$ sample.

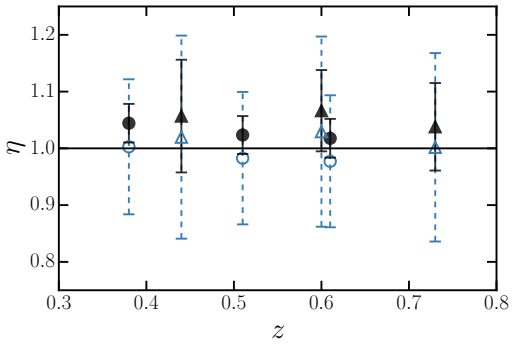

Figure 1. Marginal mean and standard deviation of η. Results with *Planck* base CPs are shown in black as filled markers with solid error bars, and those with the non-*Planck* CPs in blue as open markers with dashed error bars. Results from SNIa + BOSS are shown as circles, and those from SNIa + WiggleZ as triangles. The horizontal line marks the $\eta = 1$ case.

For the SNIa data, we generate Gaussian samples of $\mu_{\rm Lc}$ based on the compressed distance moduli described in Section 2.2. Combining them with the H_0 sample of *Planck* base CPs through Equation (6), we obtain the $d_{\rm L}$ samples.

Finally, by combining the $d_{\rm A}$ and $d_{\rm L}$ samples, we derive η through its definition in Equation (1) and generate two distinct samples from SNIa + WiggleZ and SNIa + BOSS respectively. It is worth noticing that the distance scale c/H_0 is eliminated by combining Equations (2) and (6). As a result, the distribution of η from SNIa + WiggleZ is independent of the H_0 distribution. This is not true for SNIa + BOSS, because $r_{\rm d}$ deviates from the scaling $r_{\rm d} \propto H_0^{-1}$ due to the effect of H_0 on early-Universe matter–radiation ratio (Hu et al. 1995) and recombination rates (Seager et al. 2000).

4. RESULTS

We derive constraints on η from the analysis of SNIa + BOSS and SNIa + WiggleZ samples separately. Figure 1 displays the marginal mean and standard deviation together for the purpose of visualization, but we stress again that results from different BAO surveys cannot be joined trivially.

From the SNIa + BOSS sample, using *Planck* base model CPs, we find mean and standard deviation of η as recorded in Table 2. We have used the method of batch means (Flegal et al. 2008) to verify that the MC noise affects these estimates negligibly. To check whether η sample from SNIa + WiggleZ could display skewness that may not be adequately characterized by the mean and standard deviation alone, we adopt a kernel density estimator to overcome the sampling noise in order to locate the modes of these marginal distributions along with $p = 0.683$ credibility intervals at each redshift. They are found to be $\eta(0.44) = 1.03^{+0.11}_{-0.09}$, $\eta(0.60) = 1.05^{+0.08}_{-0.06}$, and $\eta(0.73) = 1.02^{+0.08}_{-0.07}$ respectively.

These results indicate the absence of substantial evidence for deviations from Equation (1). Moreover, there is no clear trend of $\eta(z)$ evolution.

Table 2. Mean and standard deviation of η from different combinations of SNIa + BAO datasets and CP sets.

z	*Planck* base	Base + $N_{\rm eff}$ + $Y_{\rm P}$	Base + Ω_k	Non-*Planck*
SNIa + BOSS				
0.38	1.04 ± 0.03	1.04 ± 0.04	1.33 ± 0.13	1.00 ± 0.12
0.51	1.02 ± 0.03	1.02 ± 0.04	1.30 ± 0.13	0.98 ± 0.12
0.61	1.02 ± 0.03	1.01 ± 0.04	1.30 ± 0.13	0.98 ± 0.12
SNIa + WiggleZ				
0.44	1.06 ± 0.10	1.05 ± 0.10	1.34 ± 0.18	1.02 ± 0.18
0.60	1.07 ± 0.07	1.06 ± 0.08	1.35 ± 0.15	1.03 ± 0.17
0.73	1.04 ± 0.08	1.03 ± 0.08	1.31 ± 0.16	1.00 ± 0.17

The PDFs can be explored in greater detail by examining 2D joint constraints displayed in Figures 2 (SNIa + BOSS) and 3 (SNIa + WiggleZ) respectively. At different redshifts the η estimates are positively correlated, in part due to the dependence on the same and only anchoring $\mu_{\rm Lc}(z_1)$ data point.

We repeat the analysis to test the robustness of the results under different CP sets. Firstly, we switch to the *Planck* extended model with two additional free parameters, the effective number of relativistic species $N_{\rm eff}$ and the primordial ^{4}He abundance parameter $Y_{\rm P}$. The results, also recorded in Table 2 and shown as dash-dotted (green) in Figures 2 and 3, do not differ significantly from the base case. Secondly, when *Planck* chains for the base + Ω_k (spatial curvature) are used, there appears to be a preference of $\eta > 1$ as shown in the same figures as dotted (rose). However, it is known that *Planck* constraints for the curved ΛCDM model have significant tension with other cosmological probes (including the BAO and SNIa) that may be a manifestation of unresolved systematics (Grandis et al. 2016). It is for this reason that the reported deviations of η cannot be taken at face value before possible sources of conflict are identified.

Finally we consider a different CP parameterization, $\boldsymbol{\varphi}' = (H_0, \Omega_{\rm m}, f_{\rm b})$, where $f_{\rm b}$ is the baryon fraction, such that $\Omega_{\rm b} = f_{\rm b}\Omega_{\rm m}$ and the cold dark matter density $\Omega_{\rm c} = (1 - f_{\rm b})\Omega_{\rm m}$. We sample H_0 from the Gaussian distribution $h = H_0/100$ km s^{-1} Mpc^{-1} $\sim \mathcal{N}(0.688, 0.033^2)$ used in M16 based on Efstathiou (2014) and Rigault et al. (2015). The $\Omega_{\rm m}$ distribution is assumed uniform in $[0.15, 0.45]$, and $f_{\rm b}$ uniform in $[0.08, 0.20]$. The three components are generated independently. The choices of $\Omega_{\rm m}$ and $f_{\rm b}$ are inspired by studies of galaxy clusters' mass function (Bocquet et al. 2015) and baryon contents (Gonzalez et al. 2013; Chiu et al. 2016) respectively. We refer to this CP set as "non-*Planck*" for its lack of direct dependence on *Planck* assumptions or data.

In the case of SNIa + BOSS we derive the $r_{\rm d}$ distribution from $\boldsymbol{\varphi}'$ using the software CAMB (Lewis et al. 2000) following the discussions in Mehta et al. (2012) and Anderson et al. (2014). We evaluate $r_{\rm d}$ based on the fiducial ΛCDM model specified by Alam et al. (2016), but with $(H_0, \Omega_{\rm b}, \Omega_{\rm c})$ derived from the $\boldsymbol{\varphi}'$ sample rather than fixed.

Results with the non-*Planck* CPs are also displayed in Table 2 and Figures 1–3. Due to the PDF skewness, we also report the corresponding modes and credibility intervals, namely $\eta(0.38) = 1.06^{+0.07}_{-0.19}$, $\eta(0.51) = 1.04^{+0.07}_{-0.19}$, and $\eta(0.61) = 1.04^{+0.06}_{-0.19}$ (SNIa + BOSS), and $\eta(0.44) = 1.05^{+0.14}_{-0.24}$, $\eta(0.60) = 1.12^{+0.10}_{-0.26}$, and $\eta(0.73) = 1.07^{+0.11}_{-0.25}$ (SNIa + WiggleZ). Unsurprisingly, these results are less stringent than those obtained assuming the CPs tightly constrained by *Planck*.

5. DISCUSSION

In this work we have performed DD-relation tests using recent SNIa and BAO data. Assuming *Planck* base CPs we find a 3% constraint in favor of $\eta = 1$ from the analysis of SNIa + BOSS, which is consistent with weaker 7–10% constraints from SNIa + WiggleZ. In the case of non-*Planck* CPs, the results are still consistent with no DD violations at the cost of larger uncertainties (12% for SNIa + BOSS and 18% for SNIa + WiggleZ). Although nominally the constraint for $z = 0.38$ from SNIa + BOSS might be interpreted as slightly hinting at $\eta \geq 1$, at the moment it is still too preliminary to draw statistically significant conclusion from such estimate.

The work presented here differs from previous analyses not only by the use of updated data, but primarily by featuring

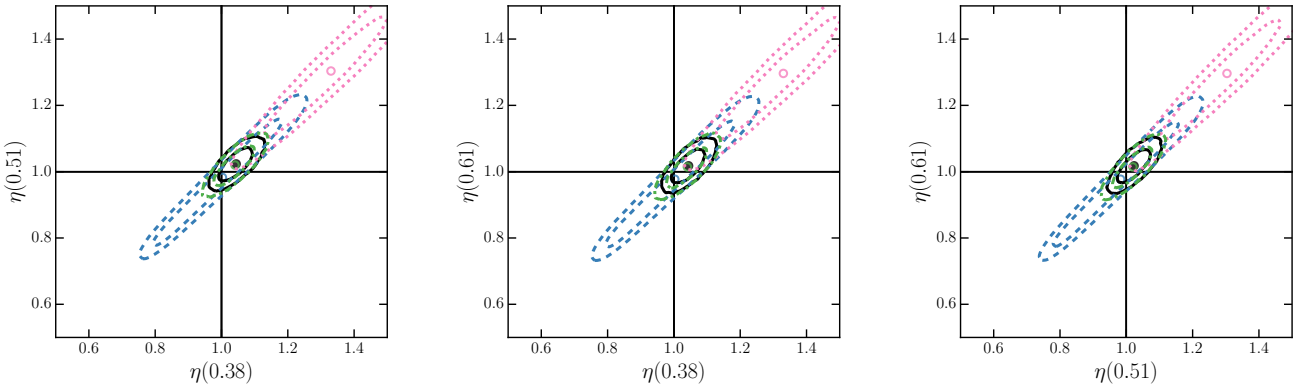

Figure 2. Two-dimensional MC distribution of η from SNIa + BOSS. Each contour set encloses an area measuring $p_1 = 0.683$ and $p_2 = 0.954$ under the corresponding PDF. Solid (black) contours show the results with *Planck* base CPs, dash-dotted (green) with *Planck* base + $N_{\rm eff}$ + $Y_{\rm P}$, dotted (rose) with *Planck* base + Ω_k, and dashed (blue) with the non-*Planck* CPs. Mean value for each case is shown by a mark of the corresponding color. Horizontal and vertical lines mark the $\eta = 1$ case. Each panel shows a 2D marginal distribution of two redshifts.

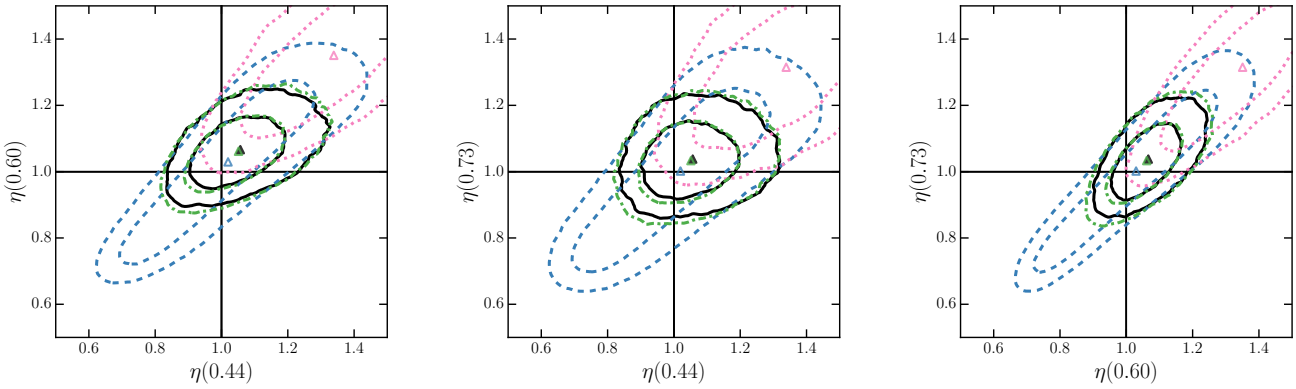

Figure 3. Similar to Figure 2 but from SNIa + WiggleZ.

new analysis methods.

Our novel SNIa compression tool (M16) produces accurate data covariance by properly treating the SNIa standardization uncertainties, in contrast to the inadequate χ^2 expression found in similar studies (e.g. Liao et al. 2015). Meanwhile, the method obviates the need to use narrow bands for redshift-matching. Compared with earlier approaches (e.g. Cardone et al. 2012; Rana et al. 2015), our compression is done in $\log_{10} z$ space where the systematic evolution of $\mu_{\rm L}$ varies less non-linearly, allowing us to use larger bandwidths. This reduces statistical uncertainties due to local sample size and is more robust against systematics of possible non-representative local sample. A similar method (Liang et al. 2013) was used with earlier Union2 SNIa data (Amanullah et al. 2010), but it did not share the aforementioned benefits and was not generalized to non-diagonal data covariance.

Another advantage of our approach concerns the estimation of errors on η, since MC sampling allows us to directly propagate the probabilistic uncertainties of the data and the CP onto η consistently, without the need of assuming Gaussian errors.

Finally, unlike previous works, our test of the DD relation does not rely on parametric constraints of artificial $\eta(z)$ evolution templates. We find indeed that no such evolution could be convincingly indicated by current data. Our method can also model faithfully the correlated uncertainty of η estimations at different redshifts, which must be taken into account if we are to investigate possible $\eta(z)$ evolution with future data. To the authors' knowledge, this is the first time the issue of template-free cross-redshift correlation is explicitly demonstrated in similar studies.

Our results stand in contrast to earlier ones from SNIa + clusters (e.g. Uzan et al. 2004; Holanda et al. 2010) or SNIa + BAO (e.g. Nair et al. 2012), in which $\eta < 1$, or anomalous SNIa brightening, was reported as being close to or above 1σ level. We suspect the origin of this seemingly unphysical conclusion might partially lie in the inadequate statistical analyses.

In this work the dependence on external parameter constraints such as *Planck*- or cluster-derived CPs are incorporated explicitly. This allows us to explore the robustness of our results under different assumptions, and to demonstrate the apparent tension between *Planck* curved ΛCDM constraints and SNIa + BAO data. Although when used jointly, regardless of possible tensions, *Planck* and BAO data point to the convergence towards a vanishing spatial curvature (Planck Collaboration et al. 2015, section 6.2.4), we stress the fact that in our analysis the BAO data and *Planck*-based CP sets are not data sources entering a joint constraint. Instead, we show that accepting the *Planck* curved ΛCDM constraints as they are will increase the SNIa–BAO tension, a conclusion complementary to the tensions studied in Grandis et al. (2016).

In the future, surveys such as *Euclid*[1] and *WFIRST*[2] will increase the data sample size and improve the study of systematic effects in cosmic distance measurements, thereby allowing us to verify the DD relation with higher precision and accuracy, and to gain insights into the physical origins of any possible violation thereof.

The data files and data-processing programs used in this work are publicly available.[3]

The research leading to these results has received funding from the European Research Council under the European Union's Seventh Framework Programme (FP/2007–2013) / ERC Grant Agreement n. 279954. CM would like to thank Antonio J. Cuesta and Bruce A. Bassett for helpful comments, and to acknowledge the support from the joint research training program of CAS and CNRS.

Software: CAMB[4] (Lewis et al. 2000), matplotlib (Hunter 2007; Droettboom et al. 2016), NumPy, and SciPy.[5]

REFERENCES

Alam, S., Ata, M., Bailey, S., et al. 2016, MNRAS, submitted, arXiv:1607.03155
Amanullah, R., Lidman, C., Rubin, D., et al. 2010, ApJ, 716, 712
Anderson, L., Aubourg, É., Bailey, S., et al. 2014, MNRAS, 441, 24
Ballinger, W. E., Peacock, J. A., & Heavens, A. F. 1996, MNRAS, 282, 877
Bassett, B. A., & Kunz, M. 2004, PhRvD, 69, 101305
Betoule, M., Kessler, R., Guy, J., et al. 2014, A&A, 568, A22
Beutler, F., Blake, C., Koda, J., et al. 2016, MNRAS, 455, 3230
Blake, C., Davis, T., Poole, G. B., et al. 2011a, MNRAS, 415, 2892
Blake, C., Glazebrook, K., Davis, T. M., et al. 2011b, MNRAS, 418, 1725
Blake, C., Brough, S., Colless, M., et al. 2012, MNRAS, 425, 405
Bocquet, S., Saro, A., Mohr, J. J., et al. 2015, ApJ, 799, 214
Cardone, V. F., Spiro, S., Hook, I., & Scaramella, R. 2012, PhRvD, 85, 123510
Chiu, I., Mohr, J., McDonald, M., et al. 2016, MNRAS, 455, 258
Corasaniti, P.-S. 2006, MNRAS, 372, 191
Crocce, M., & Scoccimarro, R. 2008, PhRvD, 77, 023533
de Bernardis, F., Giusarma, E., & Melchiorri, A. 2006, IJMPD, 15, 759
Droettboom, M., Hunter, J., Caswell, T. A., et al. 2016, matplotlib: plotting with Python, v.1.5.1, Zenodo, doi:10.5281/zenodo.44579
Efstathiou, G. 2014, MNRAS, 440, 1138
Eisenstein, D. J., Zehavi, I., Hogg, D. W., et al. 2005, ApJ, 633, 560
Ellis, G. F. R. 1971, in Proceedings of the International School of Physics "Enrico Fermi", Course 47: General Relativity and Cosmology, ed. R. K. Sachs (New York: Academic Press), 104–182
Ellis, G. F. R. 2009, GReGr, 41, 581, republication of Ellis (1971)
Etherington, I. M. H. 1933, PMag, 7, 761
—. 2007, GReGr, 39, 1055, republication of Etherington (1933)
Flegal, J. M., Haran, M., & Jones, G. L. 2008, StatSc, 23, 250
Gonzalez, A. H., Sivanandam, S., Zabludoff, A. I., & Zaritsky, D. 2013, ApJ, 778, 14
Grandis, S., Rapetti, D., Saro, A., Mohr, J. J., & Dietrich, J. P. 2016, preprint, arXiv:1604.06463
Holanda, R. F. L., Lima, J. A. S., & Ribeiro, M. B. 2010, ApJL, 722, L233
Hu, W., Scott, D., Sugiyama, N., & White, M. 1995, PhRvD, 52, 5498
Hunter, J. D. 2007, CSE, 9, 90
Lewis, A., Challinor, A., & Lasenby, A. 2000, ApJ, 538, 473
Liang, N., Li, Z., Wu, P., et al. 2013, MNRAS, 436, 1017
Liao, K., Avgoustidis, A., & Li, Z. 2015, PhRvD, 92, 123539
Ma, C., Corasaniti, P.-S., & Bassett, B. A. 2016, MNRAS, submitted, arXiv:1603.08519, (M16)
Max-Moerbeck, W., Richards, J. L., Hovatta, T., et al. 2014, MNRAS, 445, 437
Mehta, K. T., Cuesta, A. J., Xu, X., Eisenstein, D. J., & Padmanabhan, N. 2012, MNRAS, 427, 2168
Meng, X.-L., Zhang, T.-J., Zhan, H., & Wang, X. 2012, ApJ, 745, 98
Nair, R., Jhingan, S., & Jain, D. 2012, JCAP, 12, 028
Planck Collaboration, Ade, P. A. R., Aghanim, N., et al. 2015, A&A, submitted, arXiv:1502.01589
Rana, A., Jain, D., Mahajan, S., & Mukherjee, A. 2015, JCAP, accepted, arXiv:1511.09223
Rasera, Y., Corasaniti, P.-S., Alimi, J.-M., et al. 2014, MNRAS, 440, 1420
Rigault, M., Aldering, G., Kowalski, M., et al. 2015, ApJ, 802, 20
Santos-da-Costa, S., Busti, V. C., & Holanda, R. F. L. 2015, JCAP, 10, 061
Seager, S., Sasselov, D. D., & Scott, D. 2000, ApJS, 128, 407
Uzan, J.-P., Aghanim, N., & Mellier, Y. 2004, PhRvD, 70, 083533
Wu, P., Li, Z., Liu, X., & Yu, H. 2015, PhRvD, 92, 023520
Yang, X., Yu, H.-R., Zhang, Z.-S., & Zhang, T.-J. 2013, ApJL, 777, L24

[1] http://sci.esa.int/euclid/

[2] http://wfirst.gsfc.nasa.gov/

[3] http://dx.doi.org/10.5281/zenodo.57982

[4] http://camb.info/

[5] https://scipy.org/